9256 *Biochemistry* **2009,** *48,* 9256–9265
DOI: 10.1021/bi901219x

BIOCHEMISTRY
including biophysical chemistry & molecular biology
Article

Peptide Conformer Acidity Analysis of Protein Flexibility Monitored by Hydrogen Exchange[†]

David M. LeMaster,[‡] Janet S. Anderson,[§] and Griselda Hernández*,[‡]

[‡]*Wadsworth Center, New York State Department of Health, and Department of Biomedical Sciences, School of Public Health, University at Albany−SUNY, Empire State Plaza, Albany, New York 12201, and* [§]*Department of Chemistry, Union College, Schenectady, New York 12308*

Received July 16, 2009; Revised Manuscript Received August 31, 2009

ABSTRACT: The amide hydrogens that are exposed to solvent in the high-resolution X-ray structures of ubiquitin, FK506-binding protein, chymotrypsin inhibitor 2, and rubredoxin span a billion-fold range in hydroxide-catalyzed exchange rates which are predictable by continuum dielectric methods. To facilitate analysis of transiently accessible amides, the hydroxide-catalyzed rate constants for every backbone amide of ubiquitin were determined under near physiological conditions. With the previously reported NMR-restrained molecular dynamics ensembles of ubiquitin (PDB codes 2NR2 and 2K39) used as representations of the Boltzmann-weighted conformational distribution, nearly all of the exchange rates for the highly exposed amides were more accurately predicted than by use of the high-resolution X-ray structure. More strikingly, predictions for the amide hydrogens of the NMR relaxation-restrained ensemble that become exposed to solvent in more than one but less than half of the 144 protein conformations in this ensemble were almost as accurate. In marked contrast, the exchange rates for many of the analogous amides in the residual dipolar coupling-restrained ubiquitin ensemble are substantially overestimated, as was particularly evident for the Ile 44 to Lys 48 segment which constitutes the primary interaction site for the proteasome targeting enzymes involved in polyubiquitylation. For both ensembles, "excited state" conformers in this active site region having markedly elevated peptide acidities are represented at a population level that is 10^2 to 10^3 above what can exist in the Boltzmann distribution of protein conformations. These results indicate how a chemically consistent interpretation of amide hydrogen exchange can provide insight into both the population and the detailed structure of transient protein conformations.

In 1957, previous to the determination of the first protein X-ray structure, Berger and Linderstrøm-Lang (*1*) described the EX2 analysis of hydrogen exchange from structurally buried backbone amides, as summarized in the kinetic scheme:

$$\text{closed} \underset{k_{cl}}{\overset{k_{op}}{\rightleftarrows}} \text{open} \xrightarrow{k_{ch}} \text{exchanged}$$

If the rate of the closing reaction is rapid compared to the open state chemical exchange step (i.e., $k_{cl} \gg k_{ch}$), a preequilibrium of the open and closed conformational states is established, and the overall exchange rate constant k_{ex} equals $(k_{op}/k_{cl})k_{ch}$, in which k_{op}/k_{cl} is the equilibrium constant for the conformational opening transition. Since that time, the conventional steric interpretation of hydrogen exchange has held that the rate constant k_{ch} can be identified with the corresponding kinetics of exchange in model peptides, thus implying that the residual tertiary structure in the open state has no net effect on the kinetics of exchange. The ratio of the observed exchange rate to that of a corresponding model peptide can then be used to define a residue-specific free energy (i.e., $\Delta G = -RT\ln(k_{ex}/k_{pep})$) for the conformational transition(s) that give(s) rise to solvent exposure of that amide hydrogen (*2*).

The global stabilities for a number of proteins, predicted by peptide normalization of the slowest amide hydrogen exchange rates, have been independently substantiated by calorimetry or direct spectroscopic methods (*3*). However, application of the residue-specific free energy analysis to exchange processes that occur in the presence of substantial tertiary structure is more problematic. Since independent experimental data characterizing the properties of such transient partially ordered exchange-competent conformations are rarely available, the predicted residue-specific conformational free energies cannot be directly verified or refuted.

The residue-specific stability interpretation of experimental hydrogen exchange data has stimulated the development of a number of structure-based analysis algorithms (*4*−*10*) to predict the population of solvent-exposed conformations for each backbone amide. As illustrated by the widely cited COREX algorithm of Hilser and Freire (*4*), the reported success in predicting protein hydrogen exchange rates has been invoked to validate the application of this conformational sampling algorithm to a broad range of questions on protein flexibility, stability, and conformational coupling including structural propagation of ligand binding effects (*11*) and the localized energetics of allosteric coupling pathways (*12*). COREX-defined partitioning of protein structures into high, medium, and low thermodynamic stability environments (*13*) has served to characterize the determinants of fold specificity (*14*) and to structurally interpret the protein cold

[†]Financial support during manuscript preparation was provided by the National Institutes of Health (R01 GM-088214 to G.H.).

*To whom correspondence should be addressed. E-mail: griselda@wadsworth.org. Tel: 518-474-4673. Fax: 518-473-2900.

 Published on Web 09/01/2009

denaturation process (*15*) and the framework model for folding (*16*) as well as to predict the intermediate structures formed during pathological protein misfolding transitions (*17*).

Contemporaneous with the early Linderstrøm-Lang studies, Eigen (*18*) argued that amides should be "normal" acids for which the reaction rate with hydroxide ions is attenuated from the diffusion limit by the fraction of forward-reacting encounters $K_i/(K_i + 1)$, where K_i is the equilibrium constant for the transfer of a proton from the amide to an hydroxide ion. In 1972, Molday and Kallen (*19*) directly demonstrated the Eigen normal acid kinetics of amide hydrogen exchange with a diffusion-limited rate constant of 2×10^{10} M^{-1} s^{-1} at 25 °C. As a result, under EX2 kinetic conditions, measurements of hydrogen exchange offer a direct monitor of the thermodynamic acidities of the amides along the protein backbone.

A number of researchers (*20*−*25*) have pointed out that electrostatic interactions modulate the kinetics of amide hydrogen exchange. Nevertheless, many of the reported electrostatic effects have appeared to be relatively modest when compared with the 10^7−10^8-fold decrease in exchange rate that is commonly observed for the most slowly exchanging amides of moderately stable proteins. Consistent with such an assessment, it has been argued that the titrating formal charges of the side chains modulate the observed hydrogen exchange rates much more strongly via an indirect effect on protein stability than they do via a direct electrostatic interaction (*26*).

The contribution of electrostatic interactions to hydrogen exchange kinetics can be most directly addressed for the amide hydrogens that are exposed to solvent on the protein surface, since no conformational transition is required to permit the chemical exchange reaction at these sites. Recently, we (*27*, *28*) reported that the amide hydrogens which are exposed to solvent in the high-resolution X-ray structures of ubiquitin, FK506-binding protein, chymotrypsin inhibitor 2, and rubredoxin exhibit a billion-fold range in their rates of hydroxide-catalyzed exchange. The exchange rates for these amides are predictable to within a factor of 7, through the application of Poisson−Boltzmann continuum dielectric methods to the high-resolution X-ray structures.

The exchange rates of these crystallographically exposed amides are optimally predicted assuming an effective internal dielectric value of 3, despite the fact that the nonpolarizable force field atomic charge and radius parameters used in these calculations were derived by optimizing the total energies under the assumption of no background dielectric. When these crystal structure-based calculations were repeated using an internal dielectric value of 1, the slope of the predicted pK_a values for the solvent-exposed amides increased 3-fold, resulting in up to billion-fold errors in the predicted hydrogen exchange rates (*28*). Such an inverse dependence of the electrostatic free energy on the internal dielectric is directly anticipated from the generalized Born formula for an ion of charge Q and radius R (*29*):

$$\Delta G_{elec} = -(1/\varepsilon_{int} - 1/\varepsilon_{ext})Q^2/2R$$

The short lifetime of the peptide anion (~10 ps) strongly limits the dielectric shielding effects of protein conformational motion (*27*, *28*, *30*). In contrast, the conformational reorganization that occurs during the microsecond to millisecond lifetimes of side chain ionizations commonly yields effective internal dielectric values near 20 (*31*, *32*), implying roughly a 6−7-fold lower sensitivity to the electrostatic interactions of the surrounding protein structure than that observed for the peptide ionizations.

Electronic polarizability largely accounts for the dielectric shielding of the peptide anion. Refractive index measurements on typical organic liquids yield optical frequency ($\sim 10^{15}$ s^{-1}) dielectric values near 2.0. As the density within the protein interior is 30−40% higher than that of analogous small molecule organic liquids (*33*, *34*), the average contribution of electronic polarizability to the dielectric shielding of protein molecules is estimated to be at least 2.5 (*35*). On the slower time scale of $\sim 10^{-13}$ s, the nuclei respond to an altered electric field by adjusting bond lengths and angles as well as the corresponding vibrational frequencies. Although estimates vary, the nuclear relaxation response may account for as little as 5% of the total polarizability (*36*). On the other hand, larger scale conformational reorganization which occurs more slowly than the ~10 ps lifetime of the peptide anion can only weakly contribute to the observed effective dielectric shielding of the amide anions.

In considering the contribution of electronic polarizability to dielectric shielding, the macroscopic expression for the total electrostatic energy is obtained by integration of the energy density $^1/_2\varepsilon(\tau)E(\tau)^2$ over all space. In general, nonpolarizable force fields have been optimized by hyperpolarizing the charge distribution so as to reproduce the electrostatic energy of a system by a Coulombic summation in vacuo, which necessarily predicts a systematically elevated electric field intensity throughout space. Such a conflict between the predictions of energy and forces was analyzed by Feynman 70 years ago. "Many of the problems of molecular structure are concerned essentially with forces", which are treated only "indirectly through the agency of energy and its changes with changing configuration of the molecule" (*37*). As more recently emphasized by Krimm and colleagues (*38*), a molecular force field can yield correct relative electrostatic energies without correctly predicting the electrostatic forces. Such an incompatibility between predicted electrostatic forces and electrostatic energies will be most apparent across boundaries between regions having differing electrostatic representations. In enzyme QM/MM calculations, the protein interior is defined as a classical subsystem, which, when represented by an in vacuo nonpolarizable force field, can project an erroneous electrostatic potential distribution into the quantum mechanically treated active site subsystem, thus distorting the subsequent analysis of electronic structure (*28*).

Given the extreme sensitivity of the ionization of surface-exposed protein amides to the electrostatic environment, structurally buried amides that do not exchange via global unfolding might also prove to be sensitive to the electrostatic effects of the residual tertiary structure in the exchange-competent conformation. Full atom molecular dynamics methods offer the most physically robust approach for generating model representations of the Boltzmann-weighted set of conformations that characterize the flexibility of the protein native state structure. In particular, to help overcome the practical problem of incomplete conformational sampling that can limit the utility of standard unconstrained molecular dynamics protein simulations, restraints to match experimental NMR relaxation or residual dipolar coupling data can be imposed in an ensemble-averaged fashion. Ubiquitin has been widely used as a model system for the generation of such experimentally restrained conformational ensembles (*39*−*42*). To exploit the acute sensitivity of individual peptide acidities to the protein structure, an extensive set of hydrogen exchange measurements have been obtained for

ubiquitin. These data offer an experimental basis for assessing ensemble predictions of both the population and the detailed conformation of the transient exchange-competent states for this protein.

EXPERIMENTAL PROCEDURES

Protein NMR Sample Preparation. U-^{2}H,^{15}N-labeled human ubiquitin was expressed in *Escherichia coli* and purified as previously described (*28*). To facilitate optimal comparison to our previously reported magnetization transfer-based measurements of the more rapidly exchanging amides, ^{1}H exchange-in experiments were conducted. The protein sample was washed into a deuterated buffer by centrifugal ultrafiltration, and the p^{2}H was adjusted to 10 with a sodium carbonate buffer. ^{1}H,^{15}N 2D NMR correlation experiments were carried out to monitor the loss of the amide ^{1}H resonances. After back-exchange of the amide positions was completed, the protein sample was equilibrated into a ^2H_2O buffer containing 3 mM NaH_2PO_4 and 17 mM Na_2HPO_4, with sodium chloride added to a final ionic strength of 150 mM. Aliquots of 500 μL for the protein solution were then lyophilized to dryness. Immediately before NMR data collection, the protein sample was rapidly redissolved in 500 μL of 93% ^1H_2O−7% ^2H_2O and transferred to an NMR tube.

NMR Data Collection. For each ubiquitin sample, a series of ^{1}H,^{15}N 2D TROSY (*43*) spectra were collected at 25 °C on a Bruker 600 MHz NMR spectrometer. After the time interval between acquisitions of the ^{1}H exchange-in spectra increased beyond a day, CLEANEX-PM[1] (*44*, *45*) magnetization transfer-based measurements were carried out to enable direct correlation with the pH dependence of the previously reported ubiquitin CLEANEX-PM measurements (*28*).

Continuum Dielectric Calculations. Static accessibility calculations for all backbone amides were carried out on the 144 ubiquitin conformations in the 2NR2 ensemble (*40*) and the 116 protein structures in the 2K39 ensemble (*41*). In each ensemble, every amide hydrogen with a solvent-accessible surface area of at least 0.5 Å^2 in any conformation was determined with the SURFV program (*46*) using the default set of atomic radii (*47*). For each solvent-accessible residue, excepting Gln 2 which is adjacent to the positively charged N-terminus, the DelPhi Poisson−Boltzmann program (*48*) was used to predict the electrostatic potential of the amide anion for each structure in the ensemble. As an initial comparison between linear and nonlinear Poisson−Boltzmann analysis indicated negligible differences, the linear approximation was applied in this study. All other parameters for the continuum dielectric calculations were set to the values previously described (*28*). The CHARMM22 atomic charge and radius parameter set (*49*) was applied, as modified for the density functional theory-derived charge distribution of the peptide anion (*28*). Internal and solvent dielectric values of 3 and 78.5 were used. To account for the potentially rapid dielectric response of the side chain hydroxyl hydrogens, when serine and threonine residues containing gauche χ_1 side chain torsion angles have solvent-exposed amides, the side chains were modified for the intraresidue amide acidity calculation. The peptide conformer acidity for such residues was calculated according to the water dielectric equivalence assumption in which the serine side chain is truncated to alanine and the threonine side chain is truncated to α-aminobutyrate (*28*).

[1]Abbreviation: CLEANEX-PM, clean chemical exchange−phase modulated.

For each conformation in the protein ensemble, the electrostatic potential was calculated for the individual peptide anions formed by removal of the amide hydrogen from the solvent-exposed residues. To facilitate comparisons between protein amide anions in differing ensemble conformations, in each calculation an *N*-methylacetamide (or *N*-methylacetamide anion) molecule was added to the continuum dielectric lattice volume such that the distance between the *N*-methylacetamide nitrogen and the nearest formal charge was at least 16 Å and no intermolecular atomic distance was less than 8 Å (*50*). Except in the calculations summarized in Figure 2, for which only conformations exhibiting amide hydrogen solvent exposures above 0.5 Å^2 were considered, the hydrogen exchange rates were predicted by summation of the rates predicted from the conformer acidities of all solvent-exposed amide hydrogens, normalized to the number of ensemble models.

RESULTS AND DISCUSSION

Steric Accessibility Analysis of Protein Hydrogen Exchange. The billion-fold range in hydroxide-catalyzed exchange rates exhibited by the static solvent-accessible protein amides demonstrates the inadequacy of the steric accessibility model for interpretation of hydrogen exchange for this set of amides and raises concerns regarding the analysis of hydrogen exchange for structurally buried sites as well. The conventional prediction of residue-specific thermodynamic stabilities explicitly relies upon the simple criterion of exposure to solvent as determining the rate of hydrogen exchange. When combined with structural models derived from conformational sampling algorithms, the steric accessibility interpretation of hydrogen exchange has often been claimed to yield robust prediction of exchange rates for buried amides. In turn, these hydrogen exchange predictions are invoked to provide experimental verification of the conformational sampling algorithms used.

As illustrated for the hybrid structural-thermodynamic "local unfolding" model underlying the widely cited COREX algorithm (*4*), a fixed-length segment of the backbone (usually 5−12 residues) is assumed to adopt a conformationally disordered state, while the remainder of the protein maintains the crystallographic structure. The window of disordered residues is then translated along the entire length of the protein sequence so as to generate a large set of locally unfolded structures as a representation of the Boltzmann-weighted distribution of conformations that are accessible to the native state protein. In the initial COREX paper (*4*) the experimental and predicted hydrogen exchange rates for five proteins were displayed in a mirrored histogram format. Display of these data for all five proteins in a correlation plot format indicates the limited predictive capability of the COREX algorithm, as illustrated by the examples of hen lysozyme and the third domain of turkey ovomucoid (Figure 1).

Hydroxide-Catalyzed Exchange of Ubiquitin. To more fully examine the degree to which Poisson−Boltzmann continuum dielectric methods can predict the hydrogen exchange behavior of the entire set of protein amides, a complete set of experimental data is required on a protein for which the most physically realistic representations of the Boltzmann-averaged distribution of conformations are available. Drawing on the extensive molecular modeling analyses of ubiquitin and our (*28*) recent measurement of the more rapidly exchanging ubiquitin amides by magnetization transfer-based techniques, we have carried out solvent isotope exchange measurements under similar

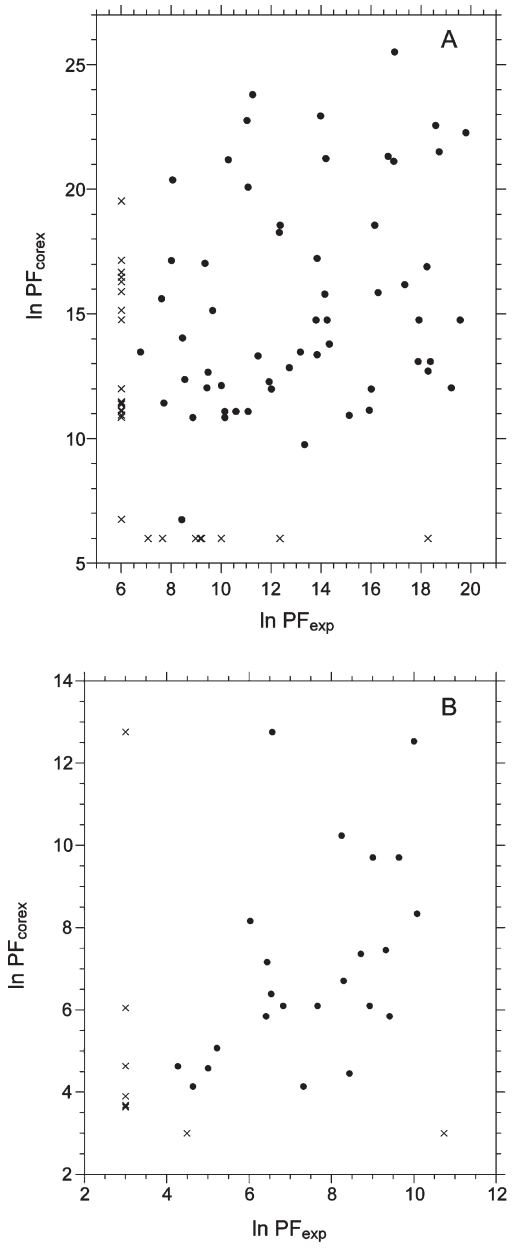

FIGURE 1: COREX predictions of hydrogen exchange for hen lysozyme and turkey ovomucoid third domain. The values as reported in the mirror histograms of Figures 3 and 7 in the COREX paper (*4*) are displayed in a correlation plot format for hen lysozyme (A) and the third domain of turkey ovomucoid (B). The experimental protection factors (PF) correspond to the ratio of exchange rate for the model peptide to that of the protein amide. For residues in which only the experimental or predicted value is reported, a cross is used to indicate that reported value.

conditions so as to provide a complementary set of exchange rate constants for the more slowly exchanging sites.

To minimize variations due to isotope effects that complicate the interpretation of conventional isotope wash-out experiments, an ^{1}H exchange-in protocol was used. By preexchange of the amide hydrogen positions with deuterium and then dissolution of the protein sample into a ^1H_2O-containing buffer, the problems of correction for the isotope dependence of solvent, buffer, and protein side chain ionizations are circumvented. By avoiding a comparison between data from normal and heavy water buffer solutions, no correction is needed for the significant differences in protein stability that can result (*51*). When compared to the earlier magnetization transfer-based hydrogen exchange measurements (*28*), the ^{1}H exchange-in protocol suffers mainly from the differential effect in breakage of an N−D or an N−H amide bond. Measurements on poly(D,L-alanine) indicate a 0.08 shift in the log rate constant for this isotope effect in the hydroxide-catalyzed exchange reaction (*52*). An additional benefit of the ^{1}H exchange-in protocol is that the final buffer conditions correspond to those used to produce the earlier reported magnetization transfer-based measurements (*28*). As a result, CLEANEX-PM experiments (*44*, *45*) could be carried out on the ^{1}H exchange-in sample so as to provide a precise calibration of the relative pH values between the two sets of measurements.

Table 1: Hydroxide-Catalyzed Rate Constants for Ubiquitin Hydrogen Exchange at 25 °C

residue	no.	log k_{OH^-}	residue	no.	log k_{OH^-}
Gln	2	6.71	Gln	41	4.91
Ile	3	0.98[a]	Arg	42	4.47
Phe	4	1.19[a]	Leu	43	5.03
Val	5	0.93[a]	Ile	44	1.33[a]
Lys	6	2.68[a]	Phe	45	3.31[a]
Thr	7	4.84	Ala	46	8.28
Leu	8	7.92	Gly	47	7.19
Thr	9	8.64	Lys	48	4.93
Gly	10	7.90	Gln	49	7.24
Lys	11	7.70	Leu	50	3.79
Thr	12	8.04	Glu	51	4.98
Ile	13	3.28[a]	Asp	52	6.43
Thr	14	6.77	Gly	53	6.94
Leu	15	0.95[a]	Arg	54	4.12
Glu	16	6.30	Thr	55	3.31[a]
Val	17	1.87[a]	Leu	56	2.35[a]
Glu	18	3.54[a]	Ser	57	5.55
Ser	20	6.46	Asp	58	5.21
Asp	21	2.06[a]	Tyr	59	3.10[a]
Thr	22	3.66	Asn	60	6.51
Ile	23	2.80[a]	Ile	61	3.89[a]
Glu	24	5.41	Gln	62	5.83
Asn	25	4.13	Lys	63	7.12
Val	26	1.52[a]	Glu	64	5.20
Lys	27	1.04[a]	Ser	65	3.88
Ala	28	3.32[a]	Thr	66	5.83
Lys	29	2.43[a]	Leu	67	3.83[a]
Ile	30	1.16[a]	His	68	4.11[a]
Gln	31	4.99	Leu	69	2.96[a]
Asp	32	5.41	Val	70	3.03[a]
Lys	33	5.89	Leu	71	6.20
Glu	34	5.03	Arg	72	7.00
Gly	35	5.41	Leu	73	7.85
Ile	36	4.41	Arg	74	8.38
Asp	39	7.17	Gly	75	8.79
Gln	40	5.67	Gly	76	7.37

[a]Log rate constant from ^{1}H exchange-in measurements at pH 7.49, 150 mM ionic strength, and 25 °C, corrected for the 0.08 difference between N−D and N−H bond cleavage (*46*). All other rate constants are from previously reported magnetization transfer-based measurements at the same temperature and ionic strength (*28*).

Table 1 lists the rate constants ($k_{OH^-} = k_{ex}/[OH^-]$) for the hydroxide-catalyzed exchange of all backbone amide hydrogens in ubiquitin at 25 °C and an ionic strength of 150 mM. We have previously reported CLEANEX-PM measurements on a series of ubiquitin samples spanning the range from pH 5.5 to pH 10.5 (*28*). As a measure of the quality of the data obtained, the static solvent-exposed amides that exhibited a simple hydroxide dependence for their exchange kinetics were fitted at multiple pH values to yield an rmsd of 0.041 for the uncertainty in their

log k_{OH^-} values. For the residues in which the ionization of the His 68 side chain (pK value of 5.92 (*53*)) alters the hydrogen exchange rate, the exchange rate constants for the neutral imidazole form of the protein were determined (*28*).

Exchange rate constants for the more slowly exchanging amides of the protein backbone were obtained from ^{1}H exchange-in measurements at pH 7.49. CLEANEX-PM measurements on this ^{1}H exchange-in sample allowed for a direct correlation to our previously reported ubiquitin exchange data. The median rmsd fit to the $(1 - \exp(-k_{ex}t))$ dependence for the amide ^{1}H peak intensities in the ^{1}H exchange-in experiments was found to be 1.2%. Only the amides of Thr 22 and Leu 50 provided robust rate constants in both sets of experimental measurements, yielding log k_{OH^-} values from the CLEANEX-PM and ^{1}H exchange-in experiments of 3.66 and 3.62 for Thr 22 as well as 3.79 and 3.67 for Leu 50.

Based on extrapolation from unfolding measurements in guanidinium chloride, transition to the EX1 kinetic condition, in which protein unfolding limits the hydrogen exchange rate, does not apply to the most slowly exchanging amides of ubiquitin in normal buffer conditions for pH values less than 9.5 (*54*). For both the CLEANEX-PM and ^{1}H exchange-in data of Table 1, the rate constant values apply to conditions in which the dominant charge state of the protein has the termini and the lysine, arginine, aspartate, and glutamate residues in the ionized state, while the His 68 side chain is neutral, as has been assumed in the previously reported ensemble calculations discussed below.

Continuum Dielectric Analysis of Highly Solvent-Exposed Amides in NMR-Restrained Ensembles. Poisson−Boltzmann continuum dielectric calculations were performed on the 144 ubiquitin structures of the NMR relaxation-restrained ensemble (PDB code 2NR2 (*40*)) and the 116 structures of the NMR residual dipolar coupling-restrained ensemble (PDB code 2K39 (*41*)). CHARMM22 atomic charge and radius parameters (*49*), to which ab initio-derived peptide anion atomic charges (*28*) were added, were input to the DelPhi program (*48*). The linearized Poisson−Boltzmann equation was applied with an internal dielectric constant of 3, the experimental ionic strength of 150 mM, and all other electrostatic parameters as previously described (*28*). To provide comparison to the earlier analysis of amides that are exposed to solvent in the high-resolution X-ray structure (*28*), peptide conformer acidities were predicted for all residues of each ensemble for which at least half of the ensemble structures have the amide hydrogen exposed to solvent by at least 0.5 Å^2 (Figure 2).

Excepting residues Gly 47 and Asp 52, the exchange kinetics of the highly exposed amides are more accurately predicted by averaging over these ensembles than by predictions using a single high-resolution X-ray structure (rmsd for log k_{OH^-} of 0.51 for 2NR2, 0.56 for 2K39, and 0.92 for the X-ray structure-based analysis (*28*)). This improvement in the conformer acidity predictions for both ensembles reflects the benefit of a physically realistic sampling of the protein conformational distribution.

In our earlier hydrogen exchange analysis of the static solvent-accessible amides of ubiquitin (*28*), it was noted that the side chain carboxylate of Asp 52 is positioned near the backbone amide of that residue in the X-ray structure (χ_1 torsion angle near −60°) which predicts a strong suppression of deprotonation for the Asp 52 nitrogen. As previously observed in the analysis of the similar case of Asp 36 in the rubredoxin from *Pyrococcus furiosus* (*27*), rotation of that side chain carboxylate to the trans rotamer increased the predicted acidity of the intraresidue amide

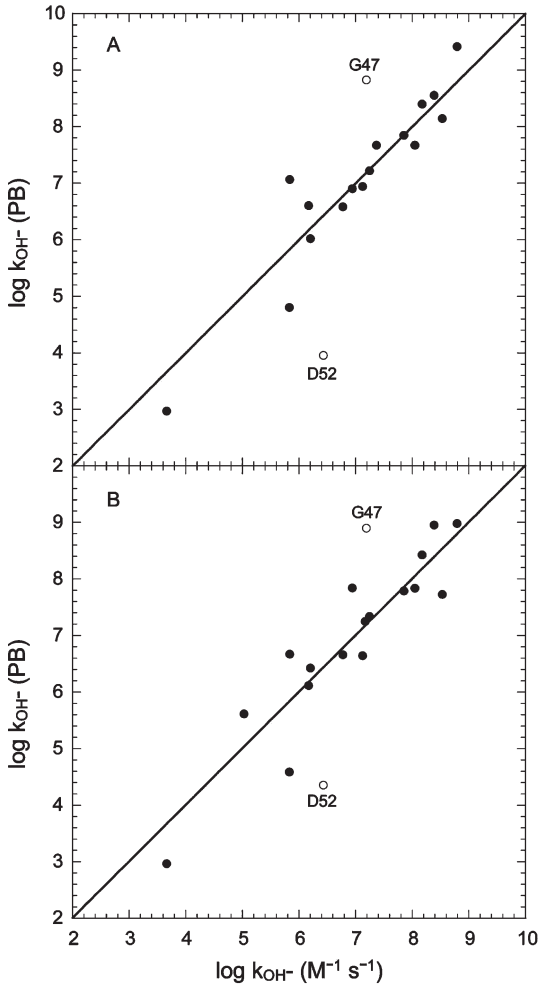

FIGURE 2: Experimental and predicted hydroxide-catalyzed rate constants for the highly exposed amides of ubiquitin. Peptide conformer acidities were predicted for residues in which the amide hydrogen is exposed to solvent by more than 0.5 Å^2 in at least 50% of the models in the NMR relaxation-restrained 2NR2 ensemble (panel A) and the NMR residual dipolar coupling-restrained 2K39 ensemble (panel B). Hydrogen exchange rate predictions were derived from the amide acidities of each conformer according to the formula (*18*) of $K_i/(K_i + 1)$ times the diffusion-limited rate of 2×10^{10} M^{-1} s^{-1} at 25 °C (*19*), where K_i is the equilibrium constant for the transfer of a proton from the amide to an hydroxide ion. The ensemble-averaged hydrogen exchange rate predictions, excluding the anomalous values for Gly 47 and Asp 52, were scaled against the experimental rates to define the y-axis intercept.

by 10^5-fold. For both of these aspartate residues, Poisson−Boltzmann predictions on the trans conformers yielded a greatly improved prediction of the experimental exchange rate.

In general, it is formally correct to calculate ionization behavior in the presence of conformational averaging by summing over the conformer acidities (i.e., $\sum K_i$) rather than the conformer pK values (i.e., $\sum pK_i$ or equivalently electrostatic potentials) (*55*). This distinction is particularly critical in the context of the comparatively weak peptide acidity since, near neutral pH, less than 1 in 10^{10} molecules will have a given amide in the ionized state. As a result, a comparatively small population of conformers with enhanced acidity can dominate the observed hydrogen exchange behavior. In the 144 structures of the 2NR2 ensemble, not a single Asp 52 side chain is predicted to occupy a trans rotamer and all except 8 of these side chain conformations have the carboxylate bound in a salt bridge to the Lys 27 side chain so that no sampling of the higher acidity conformations is

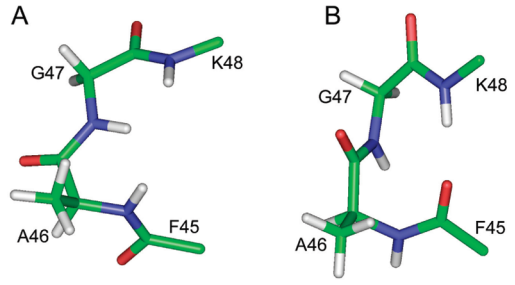

FIGURE 3: Conformation of the Phe 45 to Lys 48 ubiquitin backbone segment. Panel A is drawn from model 19 of the NMR relaxation-restrained 2NR2 ensemble (*30*), while panel B is from the X-ray structure 1UBQ (*49*).

included. In contrast, two of the three most acidic conformers for the Asp 52 amide in the 2K39 ensemble have trans χ_1 rotamers.

In Figure 3 is illustrated the structure of the backbone turn segment between Phe 45 and Lys 48 from model 19 of the 2NR2 ensemble and the corresponding segment from the X-ray structure (PDB code 1UBQ (*56*)). While the three N−H vectors point in a similar direction to help form a type III′ reverse turn in the X-ray structure (*56*), they all point inward in the ensemble model in an approximately coplanar arrangement. In addition to model 19, several other structures in both the 2NR2 and 2K39 ensembles have undergone transitions to similar local conformations for which the predicted peptide acidities for Gly 47 and Lys 48 greatly exceed the values derived from the experimental hydrogen exchange rates. The transient conformations in this region of the protein are of particular interest since residues Ile 44 to Lys 48 constitute the primary interaction surface for a wide range of enzymes that are involved in the Lys 48 polyubiquitylated signaling for proteasome degradation (*57*−*61*).

Continuum Dielectric Analysis of More Rarely Exposed Amides in an NMR Relaxation-Restrained Ensemble. Most strikingly, for the backbone amides that are exposed to solvent above 0.5 Å^2 in more than one but less than half of the models in the NMR relaxation-restrained ensemble, with the exception of Lys 48, the amide rate constant predictions are nearly as accurate (rmsd for log k_{OH^-} of 0.69) as those for the more highly exposed sites (Figure 4). Despite being structurally buried by most conventional criteria, the exchange rate constants for these 12 residues, spanning a 10^6-fold range, are predictable to within a factor of 5. With the exceptions noted above, by the experimental criterion of hydrogen exchange, the NMR relaxation-restrained ensemble 2NR2 of Vendruscolo and co-workers (*40*) appears to provide a robust representation of the Boltzmann-weighted distribution for the more highly populated protein conformations of ubiquitin.

The underestimation of the hydrogen exchange rates for residues in which only one model conformation has an amide hydrogen accessibility above 0.5 Å^2 (red symbols in Figure 4) is consistent with that expected from the statistics of undersampling. As a result of the $\sum K_i$ averaging of conformer acidities discussed above, a sufficient number of models must be sampled not only to establish the relative fraction of solvent-exposed conformations. In addition, the solvent-exposed conformations must be sufficiently sampled so as to approximate the distribution of conformer acidities therein.

The effects of undersampling the conformer acidities can be mimicked by using the median value of peptide acidity among the solvent-exposed ensemble conformations to represent the effective amide pK_a values. The resultant predictions of hydrogen

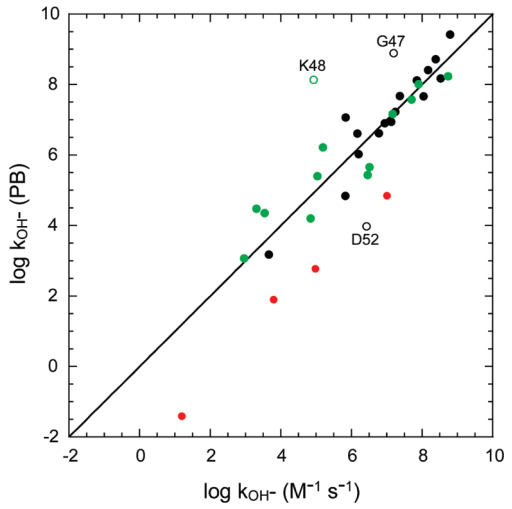

FIGURE 4: Hydroxide-catalyzed rate constants predicted from the NMR relaxation-restrained 2NR2 ensemble of ubiquitin. For residues in which the amide hydrogen is exposed to solvent by more than 0.5 Å^2 in at least one ensemble model, acidities were predicted for all conformers exhibiting any solvent exposure of the amide. Those amides which are more than 0.5 Å^2 in at least 50% of the models are marked in black. Those amides which are similarly exposed in only a single model are indicated in red, while the other transiently exposed amides are denoted in green. Residues Gly 47, Lys 48, and Asp 52 are denoted with open symbols as in Figure 2.

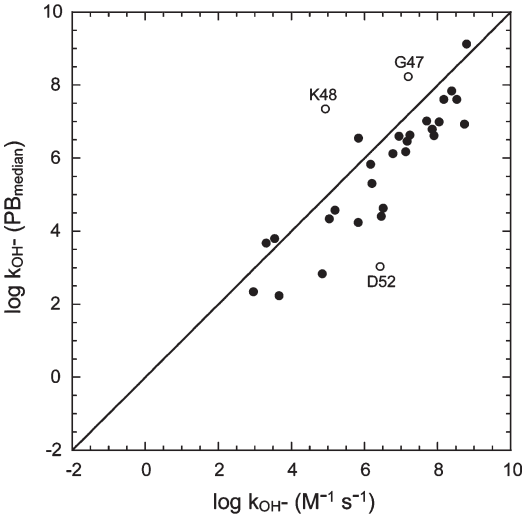

FIGURE 5: Modeling the undersampling of conformer acidities in the estimation of ubiquitin hydroxide-catalyzed rate constants. For residues in which the amide hydrogen is exposed to solvent by more than 0.5 Å^2 in more than one ensemble model, the median conformer acidity for the solvent-exposed amides was used to predict the hydrogen exchange rate constants. When compared to the experimental data, nearly all of the exchange rates were underestimated. Residues Gly 47, Lys 48, and Asp 52 are indicated by open symbols as in the figures above.

exchange rates necessarily underestimate the values derived from the correct averaging of conformer acidities for the total population of ensemble conformations. When compared to the experimentally measured exchange rates, with the notable exceptions of Gly 47 and Lys 48, nearly all of the experimental values are underestimated to a similar degree as that found for the residues with a single solvent-accessible conformation (Figure 5).

Since three of the residues illustrated in Figure 4 have only three model conformations with solvent accessibilities above 0.5 Å^2,

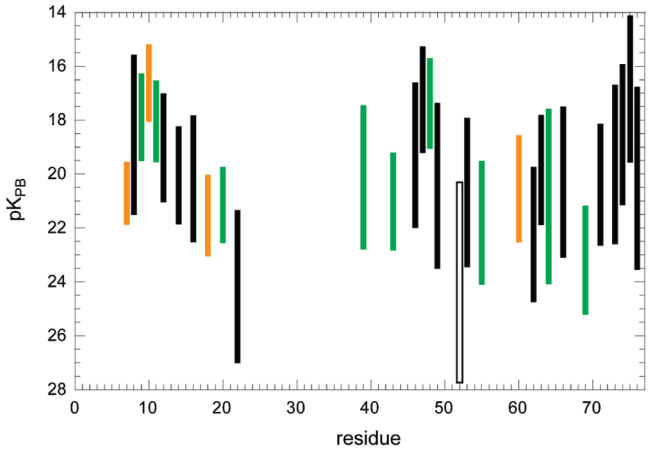

FIGURE 6: The range of conformer acidities for amide hydrogens exposed to solvent by at least 0.5 Å^2 in the NMR relaxation-restrained 2NR2 ensemble of ubiquitin. Residues for which the amide hydrogen is solvent-exposed in two to five ensemble models are indicated in orange, while those exposed to solvent in more than 50% of the models are marked in black and those with an intermediate level of exposure are shown in green. The peptide acidities are placed on an absolute scale based on their normal Eigen acid behavior, the diffusion-limited rate for hydroxide-catalyzed exchange of 2×10^{10} M^{-1} s^{-1}, and the pK of 15.7 for water at 25 °C. These properties imply an exchange rate constant of 1.0 M^{-1} s^{-1} for an amide with a pK_a value of 26.0 (*28*).

the quality of the corresponding predictions suggests that even relatively limited sampling over the set of solvent-exposed conformations may often prove to be sufficient to provide reasonable estimates of amide acidity. In this regard it should be noted that, although having at least one conformation with solvent exposure above 0.5 Å^2 was used as the criterion for inclusion of a residue in the present analysis, the acidities for all conformations having any amide hydrogen solvent exposure were used in the calculations displayed in Figure 4. In this way, the 0.5 Å^2 exposure criterion serves primarily as a filter for estimating the adequacy of statistical sampling rather than an arbitrary cutoff for contributions to the predictions of electrostatic potential. The degree of solvent exposure depends upon the atomic radius set used in the calculations, so that altering the atomic radius parameters will correspondingly alter the criterion for estimating the adequacy of statistical sampling.

The Range in Amide Conformer Acidities for Residues in the Native State. For the individual residues in which more than one 2NR2 ensemble model has an amide accessibility greater than 0.5 Å^2, the range of amide acidities for these solvent-exposed conformations varies from less than 10^3 to more than 10^7 (Figure 6). This includes the last four residues of the conformationally disordered C-terminus for which each amide exhibits at least a million-fold range in conformer acidities. As previously reported (*50*), the Ala-Ala, Gly-Ala, and Ala-Gly conformations observed in the coil regions of high-resolution X-ray structures likewise predict a million-fold range in conformer acidities which, in this case, arise predominantly from the relative orientation of the adjacent peptide units. Yet, despite this wide range in conformer acidities, summing over those dipeptide conformations from the Protein Coil Library (*62*) as a representation of the Boltzmann-weighted conformational distribution for simple model peptides accurately predicts the comparatively small differences in the experimental hydrogen exchange rates for simple Ala-Ala, Gly-Ala, and Ala-Gly model peptides (*50*). Similarly, in the present study, averaging over a million-fold range in conformer acidities yields accurate predictions of the exchange rates for the conformationally disordered C-terminus of ubiquitin. This behavior includes the amide of Gly 75 for which a significant fraction of conformers predict peptide pK_a values that are below that of water (pK_a of 15.7 at 25 °C) with the result that the effects of diffusion-limited exchange become substantial.

Many of the residues with amide hydrogen accessibilities greater than 0.5 Å^2 in the 2NR2 ensemble exhibit a range of conformer acidity values comparable to those of the conformationally disordered C-terminus, despite being considerably more restricted in the scale of their mobility. As analyzed in some detail for the hydrogen exchange study of *P. furiosus* rubredoxin (*27*), substantial contributions to the differential electrostatic potential for each static solvent-accessible amide arise from the distribution of the internal dielectric volume and the orientation of backbone partial charges, side chain partial charges, and formal charges with interaction distances ranging from van der Waals contact out to at least 14 Å. As a result, seemingly modest changes in structure surrounding a given solvent-exposed amide can give rise to large variations in the electrostatic potential and therefore in the peptide acidity at that site.

As illustration of the modest structural rearrangements which give rise to predicted hydrogen exchange in the 2NR2 ensemble for amides that are buried in the high-resolution X-ray structures, Leu 69 is the most slowly exchanging residue (log k_{OH^-} of 2.96) for which more than one ensemble model is accessible by > 0.5 Å^2. In the X-ray structures of ubiquitin, the amide of Leu 69 forms a hydrogen bond to the carbonyl oxygen of Lys 6. Three similarly acidic conformers dominate the predicted hydrogen exchange behavior for Leu 69 in the 2NR2 ensemble. When residues 2−72 of these models are superimposed on the coordinates of the X-ray structure used to initiate the NMR relaxation-restrained molecular dynamics (PDB code 1UBQ (*56*)), the backbone rmsd values were found to range from 0.57 to 0.87 Å. In each case, the distance between the position of the backbone nitrogen atom of Leu 69 in the X-ray structure as compared to the superimposed ensemble model is less than 0.4 Å. The solvent accessibility and increased peptide acidity are accompanied by an increased distance between the Leu 69 amide hydrogen and the Lys 6 oxygen to beyond 2.4 Å, while the conformation of the neighboring residues is largely unperturbed.

It should be noted that there are eight backbone amides with hydroxide-catalyzed exchange rate constants between 10^5 and 10^6 M^{-1} s^{-1} and another seven with rate constants between 10^4 and 10^5 M^{-1} s^{-1} that are not solvent accessible above 0.5 Å^2 in any of the 2NR2 ensemble models. Although the hydrogen exchange analysis illustrated in Figure 4 indicates six residues with exchange rate constants below 10^4 M^{-1} s^{-1}, these slow exchange rates predominantly reflect the weak acidities of the solvent-accessible conformers for those amides rather than the rarity of those solvent-exposed states. Under the conditions of these hydrogen exchange experiments, poly(D,L-alanine) exhibits an hydroxide-catalyzed rate constant of 2×10^8 M^{-1} s^{-1} (*63*). Given that there are only 144 conformations sampled in the 2NR2 ensemble, a buried peptide group with an exchange rate constant of 10^6 M^{-1} s^{-1} could only be expected to be represented in the present analysis if the averaged acidities of its solvent-exposed conformations were below the model peptide values.

Continuum Dielectric Analysis of More Rarely Exposed Amides in a Residual Dipolar Coupling-Restrained Ensemble. A decidedly different pattern of predicted peptide exchange rate constants results from Poisson−Boltzmann calculations on

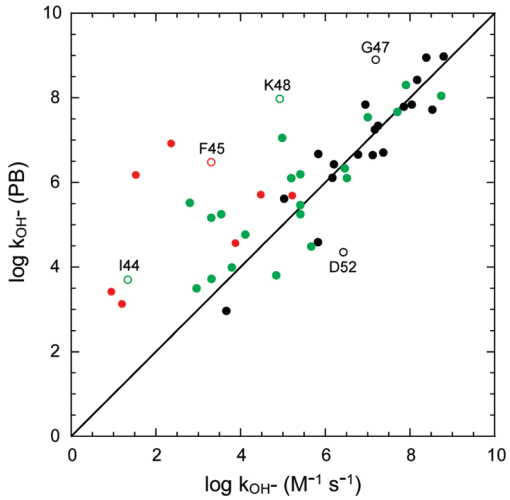

FIGURE 7: Hydroxide-catalyzed rate constants predicted from the NMR residual dipolar coupling-restrained 2K39 ensemble of ubiquitin. For residues in which the amide hydrogen is exposed to solvent by more than 0.5 Å^2 in at least one ensemble model, conformer acidities were predicted for all ensemble structures in which the amide is solvent-exposed. Those amides which are exposed by more than 0.5 Å^2 in at least 50% of the models are marked in black. Those amides which are similarly exposed in only a single model are indicated in red, while the remainder of the transiently exposed amides is denoted in green. Asp 52 and the residues involved in the primary interaction site for proteasome targeting are individually identified.

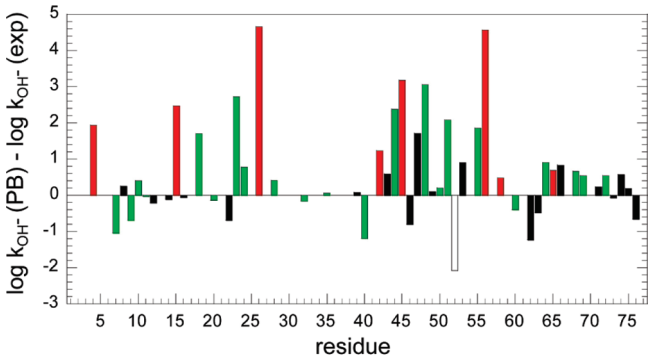

FIGURE 8: Differences in hydrogen exchange rate constants measured for ubiquitin and predicted from the NMR residual dipolar coupling-restrained 2K39 ensemble. The color coding corresponds to that used in Figure 7.

the more rarely accessible amides in the residual dipolar coupling-restrained 2K39 ensemble (Figure 7). All eight residues for which only a single ensemble model has an amide hydrogen accessibility above 0.5 Å^2 have predicted exchange rates that exceed the experimental results. As indicated in the discussion above, it is highly unlikely that all of these overestimates arise as the result of undersampling. For seven of these eight residues, the NMR relaxation-restrained 2NR2 ensemble predicts no solvent accessibility, while the predicted acidity for the one conformer with a solvent-exposed Phe 4 amide is more than 4.5 pH units higher in the 2K39 ensemble than for the 2NR2 ensemble.

In addition to the residues with a solvent-exposed amide in only a single 2K39 ensemble structure, overestimation of the hydrogen experimental amide exchange rates also occurs for a substantial fraction of the other amides which are exposed to solvent above 0.5 Å^2 in less than half of the 2K39 ensemble models. Six of these weakly exposed residues predict hydrogen exchange rates between 50- and 10^3-fold faster than observed. Among these, the amides of Ile 23 and Ile 44 are not exposed to solvent in any of the 2NR2 ensemble structures, while the amides Glu 18 and Glu 51 are much less often exposed to solvent in the 2NR2 ensemble.

The residues with backbone amides that are buried in the X-ray structures, yet have substantially overestimated hydrogen exchange rates predicted from the 2K39 ensemble, are spread throughout the ubiquitin sequence (Figure 8). Although the contribution from statistical bias due to undersampling cannot be excluded for each individual case, it is clear that the conformations with high peptide acidities for these residues in the 2K39 ensemble are greatly overrepresented, relative to the Boltzmann-weighted conformational distribution.

Of particular significance is the pattern seen for the primary proteasome targeting interaction site around residue Lys 48. The predicted log k_{OH^-} values for Ile 44, Phe 45, Gly 47, and Lys 48 exceed the experimental results by 2.4, 3.2, 1.7, and 3.1. An indication that anomalous sampling statistics do not explain these discrepancies is that for six of the seven ensemble models in which the Lys 48 amide hydrogen is exposed to solvent by more than 0.5 Å^2 each predicts a conformer hydrogen exchange rate that is more than 4000-fold above the experimentally observed value. As a result, even after normalization to the 116 models in the ensemble, the predicted exchange rate constant is significantly above the experimental value.

Although neither the amide of Ile 44 nor that of Phe 45 become solvent-exposed in any of the models in the 2NR2 ensemble, the predicted amide pK_a values of Gly 47 and Lys 48 for that ensemble also overestimate the hydrogen exchange rates for these residues to a similar degree as predicted by the 2K39 ensemble. On the other hand, the experimental S^2 order parameter values of 0.838, 0.872, 0.840, 0.821, and 0.843 for the N−H bond vectors of residues Ile 44 to Lys 48 (*64*) indicate that any internal motion, on the order of that suggested by the two conformations of Figure 3, must be very weakly populated on the picosecond to nanosecond time scale.

de Groot and colleagues (*41*) have interpreted their analysis of the residual dipolar coupling-restrained 2K39 ensemble as supporting a lock-and-key model of allostery as typically envisioned for the classical analysis of Monod, Wyman, and Changeux (*65*). More recently rechristened the population selection model, this analysis posits that the protein conformation seen in a protein−ligand complex is sufficiently highly populated in the Boltzmann-weighted conformational distribution for the apoprotein that it is kinetically efficient for the ligand to selectively collide with that conformational subpopulation in forming the resultant complex. The complementary induced fit model assumes that the ligand-bound protein conformation is relatively weakly populated in the apoprotein conformational distribution so that it is more efficient for the ligand to initially bind via a subset of interactions which then facilitate the conformational transition to the final protein−ligand complex.

One of the central aspects of distinguishing between the flexible lock-and-key and induced fit mechanisms is the accurate characterization of the Boltzmann-weighted conformational distribution. The present analysis of ubiquitin hydrogen exchange strongly indicates that the variance in conformation exhibited by the residual dipolar coupling-restrained 2K39 ensemble markedly exceeds that of the Boltzmann-weighted population. In contrast, within the limitations of the small set of 144 structures considered, the NMR relaxation-restrained 2NR2 ensemble appears to offer a substantially more robust representation of the Boltzmann-weighted conformational distribution.

CONCLUSION

The so-called protection factors that are utilized in the conventional analysis of protein hydrogen exchange simply report the alteration in the acidity of the backbone amides due to the conformational structure of the protein. What proportion of those shifts in peptide acidity arise from the free energy of the transition to an exchange-competent conformation(s) or from variations in the conformer acidities for those states can only be reliably determined by electrostatic analysis of a Boltzmann-weighted conformational distribution for that protein. Despite the various simplifications implicit in the Poisson−Boltzmann continuum dielectric analysis with nonpolarizable protein electrostatic force fields, these predictions of hydrogen exchange in ubiquitin indicate that such calculations can provide a highly effective experimental means of characterizing the reliability of various approaches to representing the conformational distribution of a protein in its native state.

Although exceptions will arise due to specific electrostatic interactions, the low dielectric shielding that characterizes the volume occupied by the residual protein structure will often cause the acidity of transiently exposed amides to be depressed below the model peptide reference values. As a result, the standard achemical steric analysis of hydrogen exchange generally underestimates the degree of conformational flexibility that is implicit in the hydrogen exchange data. As illustrated by the ensemble analyses of Phe 4 of ubiquitin, the conformational transitions that give rise to exchange of this amide appear to be underestimated by roughly 10^5-fold when the experimental hydrogen exchange data are analyzed under the steric accessibility assumption.

The NMR-restrained molecular dynamics ensembles considered in this study enable the exchange rates for the highly exposed amides of ubiquitin to be predicted to within a factor of 3 under the assumption of linear Poisson−Boltzmann analysis using CHARMM22 nonpolarizable atomic charge and radius values and an internal dielectric value of 3. This is roughly 2-fold better than the fits to experimental hydrogen exchange data for a set of four proteins analyzed using their high-resolution X-ray structures (*28*). The quality of these predictions further demonstrates both the utility of such a continuum dielectric representation for the shielding that arises predominantly from electronic polarizability and the reliability of the internal dielectric value of 3 for this representation. The great majority of enzyme QM/MM simulation studies continues to utilize nonpolarizable MM charge distributions, while biomolecular applications of polarized-embedding schemes have remained scarce (*66*). In the absence of a generally accepted polarizable classical force field of comparable accuracy, the application of an internal dielectric value of 3 can provide a robust scaling of the nonpolarizable MM electrostatic field that projects into the primary QM subsystem.

When the protein conformational transition to the exchange-competent state becomes rate-limiting for the hydrogen exchange reaction (i.e., EX1 condition), the kinetic acidity of an amide is necessarily less than its thermodynamic acidity. The formally analogous condition holds for the ionization of most carbon-bound hydrogens. As illustration, the reaction rates of nitroalkanes with hydroxide are more than 10^{10}-fold slower than that predicted for a normal Eigen acid (*67*). For such slow carbon acids, the charge delocalization that provides resonance stabilization of the anion progresses more slowly than does proton transfer (*68*), and heavy-atom intramolecular reorganization is generally the rate-limiting process (*69*). Establishing a clear physical chemistry basis for interpreting protein hydrogen exchange provides a means to characterize both the structure and the population of the protein heavy-atom reorganization processes that facilitate solvent access for the structurally buried amides.

ACKNOWLEDGMENT

We acknowledge the use of the Wadsworth Center NMR facility as well as the technical assistance of Lynn McNaughton.

REFERENCES

1. Berger, A., and Linderstrøm-Lang, K. (1957) Deuterium exchange of poly-DL-alanine in aqueous solution. *Arch. Biochem. Biophys. 69*, 106–118.
2. Bai, Y., Milne, J. S., Mayne, L., and Englander, S. W. (1994) Protein stability parameters measured by hydrogen exchange. *Proteins 20*, 4–14.
3. Huyghues-Despointes, B. M. P., Scholtz, J. M., and Pace, C. N. (1999) Protein conformational stabilities can be determined from hydrogen exchange rates. *Nat. Struct. Biol. 6*, 910–912.
4. Hilser, V. J., and Freire, E. (1996) Structure-based calculations of the equilibrium folding pathway of proteins. Correlation with hydrogen exchange protection factors. *J. Mol. Biol. 262*, 756–772.
5. Wallqvist, A., Smythers, G. W., and Covell, D. G. (1997) Identification of cooperative folding units in a set of native proteins. *Protein Sci. 6*, 1627–1642.
6. Bahar, I., Wallqvist, A., Covell, D. G., and Jernigan, R. L. (1998) Correlation between native-state hydrogen exchange and cooperative residue fluctuations from a simple model. *Biochemistry 37*, 1067–1075.
7. Sheinerman, F. B., and Brooks, C. L., III (1998) Molecular picture of folding of a small α/β protein. *Proc. Natl. Acad. Sci. U.S.A. 95*, 1562–1567.
8. Garcia, A. E., and Hummer, G. (1999) Conformational dynamics of cytochrome *c*: Correlation to hydrogen exchange. *Proteins: Struct., Funct., Genet. 36*, 175–191.
9. Dixon, R. D. S., Chen, Y., Ding, F., Khare, S. D., Prutzman, K. C., Schaller, M. D., Campbell, S. L., and Dokholyan, N. V. (2004) New insights into FAK signaling and localization based on detection of a FAT domain folding intermediate. *Structure 12*, 2161–2171.
10. Livesay, D. R., Dallakyan, S., Wood, G. G., and Jacobs, D. J. (2004) A flexible approach for understanding protein stability. *FEBS Lett. 576*, 468–476.
11. Freire, E. (1999) The propagation of binding interactions to remote sites in proteins: Analysis of the binding of the monoclonal antibody D1.3 to lysozyme. *Proc. Natl. Acad. Sci. U.S.A. 96*, 10118–10122.
12. Pan, H., Lee, J. C., and Hilser, V. J. (2000) Binding sites in *Escherichia coli* dihydrofolate reductase communicate by modulating the conformational ensemble. *Proc. Natl. Acad. Sci. U.S.A. 97*, 12020–12025.
13. Wrabl, J. O., Larson, S. A., and Hilser, V. J. (2001) Thermodynamic propensities of amino acids in the native state ensemble: Implications for fold recognition. *Protein Sci. 10*, 1032–1045.
14. Wrabl, J. O., Larson, S. A., and Hilser, V. J. (2002) Thermodynamic environments in proteins: Fundamental determinants of fold specificity. *Protein Sci. 11*, 1945–1957.
15. Babu, C. R., Hilser, V. J., and Wand, A. J. (2004) Direct access to the cooperative substructure of proteins and the protein ensemble via cold denaturation. *Nat. Struct. Mol. Biol. 11*, 352–357.
16. Wang, S. W., Gu, J., Larson, S. A., Whitten, S. T., and Hilser, V. J. (2008) Denatured-state energy landscapes of a protein structural database reveal the energetic determinants of a framework model for folding. *J. Mol. Biol. 381*, 1184–1201.
17. Cremades, N., Sancho, J., and Freire, E. (2006) The native-state ensemble of proteins provides clues for folding, misfolding and function. *Trends Biochem. Sci. 31*, 494–496.
18. Eigen, M. (1964) Proton transfer, acid-base catalysis, and enzymatic hydrolysis. (I) Elementary processes. *Angew. Chem., Int. Ed. 3*, 1–19.
19. Molday, R. S., and Kallen, R. G. (1972) Substituent effects on amide hydrogen exchange rates in aqueous solution. *J. Am. Chem. Soc. 94*, 6739–6745.
20. Kim, P. S., and Baldwin, R. L. (1982) Influence of charge on the rate of amide proton exchange. *Biochemistry 21*, 1–5.
21. Tüchsen, E., and Woodward, C. (1985) Hydrogen kinetics of peptide amide protons at the bovine pancreatic trypsin inhibitor protein-solvent interface. *J. Mol. Biol. 185*, 405–419.

22. Delepierre, M., Dobson, C. M., Karplus, M., Poulsen, F. M., States, D. J., and Wedin, R. E. (1987) Electrostatic effects and hydrogen exchange behavior in proteins. The pH dependence of exchange rates in lysozyme. *J. Mol. Biol. 197*, 111–122.
23. Dempsey, C. E. (1995) Hydrogen bond stabilities in the isolated alamethicin helix: pH-dependent amide exchange measurements in methanol. *J. Am. Chem. Soc. 117*, 7526–7534.
24. Forsyth, W. R., and Robertson, A. D. (1996) Intramolecular electrostatic interactions accelerate hydrogen exchange in diketopiperazine relative to 2-piperidone. *J. Am. Chem. Soc. 118*, 2694–2698.
25. Fogolari, F., Esposito, G., Viglino, P., Briggs, J. M., and McCammon, J. A. (1998) pK_a shift effects on backbone amide base-catalyzed hydrogen exchange rates in peptides. *J. Am. Chem. Soc. 120*, 3735–3738.
26. Matthew, J. B., and Richards, F. M. (1983) The pH dependence of hydrogen exchange in proteins. *J. Biol. Chem. 258*, 3039–3044.
27. Anderson, J. S., Hernández, G., and LeMaster, D. M. (2008) A billion-fold range in acidity for the solvent-exposed amides of *Pyrococcus furiosus* rubredoxin. *Biochemistry 47*, 6178–6188.
28. Hernández, G., Anderson, J. S., and LeMaster, D. M. (2009) Polarization and polarizability assessed by protein amide acidity. *Biochemistry 48*, 6482–6494.
29. Schaefer, M., and Karplus, M. (1996) A comprehensive analytical treatment of continuum electrostatics. *J. Phys. Chem. 100*, 1578–1599.
30. LeMaster, D. M., Anderson, J. S., and Hernández, G. (2007) Spatial distribution of dielectric shielding in the interior of *Pyrococcus furiosus* rubredoxin as sampled in the subnanosecond timeframe by hydrogen exchange. *Biophys. Chem. 129*, 43–48.
31. Antosiewicz, J., McCammon, J. A., and Gilson, M. K. (1996) The determinants of pK_as in proteins. *Biochemistry 35*, 7819–7833.
32. Demchuk, E., and Wade, R. C. (1996) Improving the continuum dielectric approach to calculating pK_a's of ionizable groups in proteins. *J. Phys. Chem. 100*, 17373–17387.
33. Richards, F. M. (1974) The interpretation of protein structures: Total volume, group volume distributions and packing density. *J. Mol. Biol. 82*, 1–14.
34. Tsai, J., Taylor, R., Chothia, C., and Gerstein, M. (1999) The packing density in proteins: Standard radii and volumes. *J. Mol. Biol. 290*, 253–266.
35. Mertz, E. L., and Krishtalik, L. I. (2000) Low dielectric response in enzyme active site. *Proc. Natl. Acad. Sci. U.S.A. 97*, 2081–2086.
36. Hawranek, J. P., Wrzeszcz, W., Muszyński, A. S., and Pajdowska, M. (2002) Infrared dispersion of liquid triethylamine. *J. Non-Cryst. Solids 305*, 62–70.
37. Feynman, R. P. (1939) Forces in molecules. *Phys. Rev. 56*, 340–343.
38. Palmo, K., Mannfors, B., Mirkin, N. G., and Krimm, S. (2006) Inclusion of charge and polarizability fluxes provides needed physical accuracy in molecular mechanics force fields. *Chem. Phys. Lett. 429*, 628–632.
39. Lindorff-Larsen, K., Best, R. B., DePristo, M. A., Dobson, C. M., and Vendruscolo, M. (2005) Simultaneous determination of protein structure and dynamics. *Nature 433*, 128–132.
40. Richter, B., Gsponer, J., Varnai, P., Salvatella, X., and Vendruscolo, M. (2007) The MUMO (minimal under-restraining minimal over-restraining) method for the determination of native state ensembles of proteins. *J. Biomol. NMR 37*, 117–135.
41. Lange, O. F., Lakomek, N. A., Fares, C., Schroder, G. F., Walter, K. F. A., Becker, S., Meiler, J., Grubmuller, H., Griesinger, C., and deGroot, B. L. (2008) Recognition dynamics up to microseconds revealed from an RDC-derived ubiquitin ensemble in solution. *Science 320*, 1471–1475.
42. DeSimone, A., Richter, B., Salvatella, X., and Vendruscolo, M. (2009) Toward an accurate determination of free energy landscapes in solution states of proteins. *J. Am. Chem. Soc. 131*, 3810–3811.
43. Pervushin, K., Riek, R., Wider, G., and Wüthrich, K. (1997) Attenuated T2 relaxation by mutual cancellation of dipole-dipole coupling and chemical shift anisotropy indicates an avenue to NMR structures of very large biological macromolecules. *Proc. Natl. Acad. Sci. U.S.A. 94*, 12366–12371.
44. Hwang, T. L., vanZijl, P. C. M., and Mori, S. (1998) Accurate quantitation of water-amide proton exchange rates using the phase-modulated CLEAN chemical EXchange (CLEANEX-PM) approach with a fast-HSQC (FHSQC) detection scheme. *J. Biomol. NMR 11*, 221–226.
45. Hernández, G., and LeMaster, D. M. (2003) Relaxation compensation in chemical exchange measurements for the quantitation of amide hydrogen exchange in larger proteins. *Magn. Reson. Chem. 41*, 699–702.
46. Sridharan, S., Nicholls, A., and Honig, B. (1992) A new vertex algorithm to calculate solvent accessible surface-areas. *Biophys. J. 61*, A174.
47. Rashin, A. A. (1984) Buried surface area, conformational entropy, and protein stability. *Biopolymers 23*, 1605–1620.
48. Rocchia, W., Sridharan, S., Nicholls, A., Alexov, E., Chiabrera, A., and Honig, B. (2002) Rapid grid-based construction of the molecular surface and the use of induced surface charge to calculate reaction field energies: Applications to the molecular systems and geometric objects. *J. Comput. Chem. 23*, 128–137.
49. MacKerell, A. D., Jr., Bashford, D., Bellott, M., Dunbrack, R. L., Jr., Evanseck, J. D., Field, M. J., Fischer, S., Gao, J., Guo, H., Ha, S., Joseph-McCarthy, D., Kuchnir, L., Kuczera, K., Lau, F. T. K., Mattos, C., Michnick, S., Ngo, T., Nguyen, D. T., Prodhom, B., Reiher, W. E.III, Roux, B., Schlenkrich, M., Smith, J. C., Stote, R., Straub, J., Watanabe, M., Wiorkiewicz-Kuczera, J., Yin, D., and Karplus, M. (1998) All-atom empirical potential for molecular modeling and dynamics studies of proteins. *J. Phys. Chem. B 102*, 3586–3616.
50. Anderson, J. S., Hernández, G., and LeMaster, D. M. (2009) Backbone conformational dependence of peptide acidity. *Biophys. Chem. 141*, 124–130.
51. Makhatadze, G. I., Clore, G. M., and Gronenborn, A. M. (1995) Solvent isotope effect and protein stability. *Nat. Struct. Biol. 2*, 852–855.
52. Connelly, G. P., Bai, Y. W., Jeng, M. F., and Englander, S. W. (1993) Isotope effects in peptide group hydrogen-exchange. *Proteins 17*, 87–92.
53. Ibarra-Molero, B., Loladze, V. V., Makhatadze, G. I., and Sanchez-Ruiz, J. M. (1999) Thermal versus guanidine-induced unfolding of ubiquitin. An analysis in terms of the contributions from charge-charge interactions to protein stability. *Biochemistry 38*, 8138–8149.
54. Sivaraman, T., Arrington, C. B., and Robertson, A. D. (2001) Kinetics of unfolding and folding from amide hydrogen exchange in native ubiquitin. *Nat. Struct. Biol. 8*, 331–333.
55. You, T. J., and Bashford, D. (1995) Conformation and hydrogen ion titration of proteins: A continuum electrostatic model with conformational flexibility. *Biophys. J. 69*, 1721–1733.
56. Vijay-Kumar, S., Bugg, C. E., and Cook, W. J. (1987) Structure of ubiquitin refined at 1.8 Å resolution. *J. Mol. Biol. 194*, 531–544.
57. Fisher, R. D., Wang, B., Alam, S. L., Higginson, D. S., Robinson, H., Sundquist, W. I., and Hill, C. P. (2003) Structure and ubiquitin binding of the ubiquitin-interacting motif. *J. Biol. Chem. 278*, 28976–28984.
58. Ponting, C. P. (2000) Proteins of the endoplasmic-reticulum-associated degradation pathway: domain detection and function prediction. *Biochem. J. 351*, 527–535.
59. Alam, S. L., Sun, J., Payne, M., Welch, B. D., Blake, B. K., Davis, D. R., Meyer, H. H., Emr, S. D., and Sundquist, W. I. (2004) Ubiquitin interactions of NZF zinc fingers. *EMBO J. 23*, 1411–1421.
60. Wang, Q., Goh, A. M., Howley, P. M., and Walters, K. J. (2003) Ubiquitin recognition by the DNA repair protein hHR23a. *Biochemistry 42*, 13529–13535.
61. Wang, B., Alam, S. L., Meyer, H. H., Payne, M., Stemmler, T. L., Davis, D. R., and Sundquist, W. I. (2003) Structure and ubiquitin interactions of the conserved zinc finger domain of Npl4. *J. Biol. Chem. 278*, 20225–20234.
62. Fitzkee, N. C., Fleming, P. J., and Rose, G. D. (2005) The Protein Coil Library: A structural database of nonhelix, nonstrand fragments derived from the PDB. *Proteins 58*, 852–854.
63. Bai, Y., Milne, J. S., Mayne, L., and Englander, S. W. (1993) Primary structure effects on peptide group hydrogen-exchange. *Proteins: Struct., Funct., Genet. 17*, 75–86.
64. Tjandra, N., Feller, S. E., Pastor, R. W., and Bax, A. (1995) Rotational diffusion anisotropy of human ubiquitin from ^{15}N NMR relaxation. *J. Am. Chem. Soc. 117*, 12562–12566.
65. Monod, J., Wyman, J., and Changeux, J. P. (1965) On the nature of allosteric transitions: A plausible model. *J. Mol. Biol. 12*, 88–118.
66. Senn, H. M., and Thiel, W. (2009) QM/MM methods for biomolecular systems. *Angew. Chem., Int. Ed. 48*, 1198–1229.
67. Bordwell, F. G., Boyle, W. J., and Yee, K. C. (1970) Equilibrium and kinetic acidities of nitroalkanes and their relationship to transition state structures. *J. Am. Chem. Soc. 92*, 5926–5932.
68. Bernasconi, C. F. (1987) Intrinsic barriers of reactions and the principle of nonperfect synchronization. *Acc. Chem. Res. 20*, 301–308.
69. Costentin, C., and Saveant, J. M. (2004) Why are proton transfers at carbon slow? Self-exchange reactions. *J. Am. Chem. Soc. 126*, 14787–14795.